OPTIMIZATION AND ANALYSIS OF THE MODIFIED PLVL-VARIABLE STIFFNESS ACTUATOR

M. Dežman A. Gams

Department of Automation, Biocybernetics and Robotics, Jožef Stefan Institute, Jamova 39, 1000 Ljubljana, Slovenia, Jožef Stefan International Postgraduate School, Jamova 39, 1000 Ljubljana, Slovenia

ABSTRACT

The pseudo-linear variable-stiffness actuator (PLVL-VSA) is a variable stiffness actuator with a mechanical stiffness adaptation. It has a nearly linear torque deflection characteristics and an energy efficient stiffness variation. However, this stiffness variation efficiency is reduced at higher mechanism deflections, which manifests as a higher torque required to retain the desired mechanism's stiffness. In this work, a modification that decreases the stiffness varying motor torque, thus increasing mechanism's energy efficiency, is proposed. The main design parameters are optimized with respect to the highest torque/deflection workspace, while staying below the peak torque constraints of both motors' gearboxes. The effect of the modification is analysed and compared to the original mechanism. The new configuration requires less torque and energy to vary the stiffness compared to the original mechanism in a slightly reduced mechanism stiffness range.

Keywords: variable-stiffness mechanism, energy-efficient, stiffness variation, parameter optimization, workspace increase

1 INTRODUCTION

Hardware with mechanical compliance introduces several benefits for robotic applications both from the robot's and user's perspective. These include safer human-robot interaction and better movement energy efficiency [1]. The compliant element is a low-pass filter [2] that reduces the peak forces; it therefore protects the mechanical components of the device. Improved force accuracy in higher stability is another advantage. As a disadvantage, the control bandwidth of the actuator is reduced. The mechanical complexity is higher compared to classical plain geared motors, which makes them harder to use and implement. However, this is also why there are many opportunities for mechanical simplification and control design research [3]. Researchers focus on novel device architectures

Contact author: M. Dežman¹, A. Gams¹

¹Jožef Stefan Institute, Jamova 39, 1000 Ljubljana, Slovenia E-mail: miha.dezman@ijs.si , andrej.gams@ijs.si

development and prototype manufacturing, also due to the commercial unavailability of such devices. Many different types of compliant mechanisms with different advantages and disadvantages consequently exist in the literature [4], [5] and [6].

The subgroup of Variable Stiffness Actuators (VSA) employ a special mechanism, that can physically vary the mechanical compliance of the device often with the use of a secondary motor. These VS mechanisms or actuators are already implemented in some walking, jumping and humanoid robots. Using them, one can, e.g., adapt the natural frequency of the mechanism [7]. In the DLR Hand-Arm System [8], which will be part of a humanoid robot, VSA compliant actuators are the tightly integrated in all of its joints. Another example is the jumping robot SALTO that is capable of higher jumps by storing energy in its elastic element [9].

Wearable devices are another interesting area, where often a specific stiffness is desired, and where a variable stiffness mechanism could provide it. In rehabilitation robotics, the variable stiffness elastic elements can provide different levels of assistance and gravity compensation. Such an exoskeleton is the HARMONY, which utilizes a cable transmission

with specially designed pulleys in combination with springs to passively compensate for gravity loads [10]. Another case is the passive-ankle exoskeleton [11], which is able to reduce the users walking effort in a passive manner using a spring in combination with a clutch. The device produces optimal results at a specific stiffness. Here, a variable stiffness mechanism could adapt the stiffness for optimal performance. Another interesting use-case represent the exoskeletons for overhead work, which are getting increasingly popular in industry [12, 13, 14]. A variable stiffness mechanism could adapt its stiffness based on the users arm posture or the weight of different hand-tools used. Through this, the device could completely passively compensate for the loads. It can be seen that not only is the development of compliant actuators important, but also the development of underlying compliant mechanisms.

This work is the development continuation of a novel variable stiffness actuator principle first presented in [15]. Later, this principle was upgraded in [16]. In both works, the mechanism's high stiffness variation efficiency stands out. A drawback of the proposed design is the efficiency decrease at higher mechanism deflections. It is a drawback, because it limits the useful torque/deflection workspace of the mechanism. This manuscript proposes a modification, which reduces the stiffness variation torque and thus preserves the stiffness variation efficiency even at higher mechanism deflections.

The manuscript is organized as follows. Section 2 serves to re-introduce the PLVL-VSA mechanism. The main operation principle is explained (Sec. 2.1), together with its properties (Sec. 2.2) and difficulties (Sec. 2.3). The proposed modification is explained in Section 3, including the new mathematical model. The optimization of the parameters aimed to achieve optimal performance, is shown in Section 4. The section begins with the introduction of the optimization goal (Sec. 4.1) and its cost function (Sec. 4.2). The cost function is then evaluated (Sec. 4.3) and the results analysed (Sec. 4.5). The article is concluded in Section 5 with a short overall summary. APPENDIX A gathers the less important equations used throughout the article.

2 VARIABLE STIFFNESS MECHANISM

2.1 THE PLVL-VSA

For brevity, this section describes the original mechanism's operation principle, which was initially proposed in a simplified form in [15]. The initial version was manufactured using rapid prototyping technologies, consequently, the mechanism could operate only at smaller loads. The actuator was then redesigned into a more durable form and prepared for integration into an elbow exoskeleton device [16].

The basic principle of operation is a combination of a variable lever principle and a cam mechanism. The essential components are shown in Fig. 1(a). The rotation/deflection

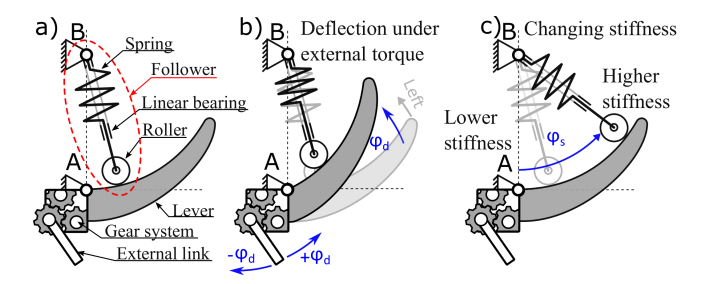


Figure 1 The VSA working principle: a) at equilibrium position, b) deflected, and c) varying the stiffness.

of the curved lever around the pivot A (increasing the deflection angle φ_d) compresses the linear spring (Fig. 1b). The lever is connected to the external link to which it provides the reaction torque, either directly, if a one directional compression is sufficient, or indirectly, if a bidirectional compression is needed. The rotation of the follower (Fig.1a) around the pivot B, changes the effective radius between the spring and the pivot A (Fig. 1c). This increases the force needed to compress the spring and makes the mechanism a variable stiffness mechanism.

The deflection arm has an arc shape, this way, the spring system can be rotated ideally without resistance, since the force/torque needed to vary the stiffness is applied perpendicularly to the load. This results in an energy efficient stiffness variation. A higher follower angle (φ_s) results in a higher stiffness of the mechanism. The reader should not misunderstand that while in some graphs only a few follower angles are chosen for clarity, the stiffness of the mechanism can be changed continuously and under all loads, as long as they are below the peaks of both motors' gearboxes. To elaborate, two motors are utilized in this case. The first motor is the position motor placed at pivot A and is tasked to change the equilibrium or position of the external link. The second, ideally a less powerful one compared to the position motor, is placed at pivot B and tasked to change the mechanism's stiffness.

In principle, the mechanism's functioning is one directional, meaning that it can be compressed only. To achieve a bidirectional application, a special transmission mechanism is needed to change the bidirectional motion of the external link to a one-directional compression movement of the curved lever. Such mechanism variants are explained in [15] using gears and in [16] using cables. Since the bidirectional mechanism is not directly related to the efficiency of variable stiffness mechanism in question, it is omitted in this article.

2.2 MECHANISM PROPERTIES

The PLVL-VSA mechanism has several advantages. The first advantage lies in the fact, that the stiffness variation is achieved in a perpendicular fashion. Consequently, most of the stiffness varying motor energy is used to vary the stiffness. In contrast, if the stiffness is varied in parallel with the elastic element, some energy is needed to overcome

the spring pretension, as described in [17]. Consequently, a stronger and therefore also a bigger motor is needed to achieve the same stiffness variation speed. An efficient stiffness variation not only saves electric energy, but also reduces overall weight, since the stiffness variation motor can be smaller.

The flat geometrical structure is also considered an advantage, since the 2D geometry of most parts enables cheaper manufacture. It might also be a more suitable solution for wearable devices, since it keeps the components closer to the human body. The next important feature is the pseudo-linear torque/deflection characteristics.

To explain it, the Fig. 2 needs to be introduced. The graph shows amount of torque needed to compress the mechanism at different follower angles. The equations needed to draw it,

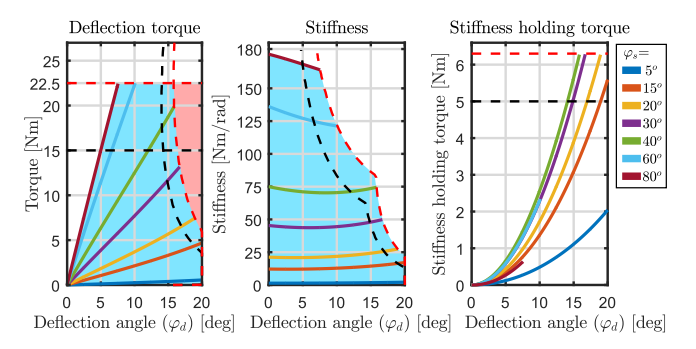


Figure 2 The *left* graph shows the torque-deflection characteristic. The *middle* graph shows the corresponding derivative, i.e., stiffness. The stiffness holding torque required to hold a given follower angle is show in *right*. The BLUE region represents the below peak operation space of both motors. On the other hand, the RED region represents the area with the stiffness holding motor torques above its peak torque limit. The solid lines correspond to different follower angles as seen in the legend. The black and red dashed lines represent the nominal and peak torques of the position and stiffness varying motor gearboxes.

are summarized in the APPENDIX A, whereas the original derivations can be found in [16]. In short, the $\tau_{\rm d,F1}$ (36) is used to draw the torque lines. The stiffness is calculated using $K_{\rm d,F1}$ (37) and the required stiffness holding torque as $\tau_{\rm s,F1}$ (39). All parameters used are gathered in Table I. The red dashed and black dashed lines represent the limits and boundaries between the nominal and peak/maximum torques of the actuator's motors, respectively. They are determined via the trimming of the torque/deflection curves by the torque limits in a numerical fashion. With the use of motor/gearbox torque limits found in Table I, the torque-deflection workspace (Fig. 2) is split into several distinctly coloured areas. For practical reasons, all curves, except for the deflection torque and stiffness holding torque, are calculated numerically.

In the BLUE area, both of the motors are operating below their specified peak torques. The RED area is created,

Table I - Calculation parameters

Variable	Name	Value	Unit
$R_{ m s}$	Cam parameter 1	50	[mm]
R_{b}	Cam parameter 2	0	[mm]
k_{lin1}	Linear spring stiffness	72.6	[N/mm]
$arphi_{ m d}$	Deflection angle range	± 20	[°]
φ_{s}	Stiff. follower angle	0 - 90	[°]
$P_{\rm s}$	Stiff. varying mot. power	20	[W]
$T_{\rm sn}, {T_{\rm sp}}^*$	Stiff. varying mot. limits	5, 6.3	[Nm]
P_{p}	Position motor power	80	[W]
$T_{\rm pn}, T_{\rm pp}^*$	Position motor limits	15, 22.5	[Nm]

*The values pn, pp, sn and sp stand for position nominal, position peak, stiffness nominal and stiffness peak, respectively.

when the torque limits of the stiffness variation motor is mapped into the torque/deflection workspace. In the RED area, the actual torque requirements exceeds the maximum torque capabilities of the stiffness variation motor. Since the position motor can be back-driven above its peak torque, this essentially creates the WHITE area above the BLUE area, which theoretically can not be accessed.

Finally, observe that the lines of the torque appear almost linear, i.e. pseudo-linear, and can thus be described by a linear approximation in sufficient precision. The mechanism's behaviour at each follower angle can thus be described with one parameter only, i.e. the equivalent linear stiffness. This property is considered an important advantage, for our task, for two reasons.

Firstly, because it enables the use of a simplified control algorithm. The algorithm described in [2] can directly be applied, since the actuators response is linear. Secondly, because it enables an easy comparison between possible modifications by using the equivalent stiffness as a baseline. It must be noted, that while our task benefits from a linear characteristics, some applications benefit from a nonlinear characteristic. One such example is the stiffness of an ankle prosthesis [18]. However, in such an example, the stiffness requires more than one parameter to be described and depends on the stiffness setup parameter and the deflection of the mechanism, i.e., two parameters or more. This also calls for a more unconventional and more complex non-linear control design, like in [19] where authors use a VSA with a non-linear characteristics.

When the curved arm deviates from the equilibrium position, a tangential force appears due to the rising pressure angle of the cam mechanism. This force is calculated in equation (38) found in APPENDIX A. The stiffness variation motor has to overcome this force/torque in order to vary the stiffness. It is considered as the prime reason for the decrease of the efficiency of the stiffness variation and as a potential disadvantage of the mechanism. At higher deflection angles and lower follower angles, this force and the problem becomes even more prominent. We call this problem also as the rising follower torque, i.e., stiffness holding torque

at lower follower angles and larger deflections, since it is directly connected to the amount of torque the stiffness variation motor requires. The torque required to retain the stiffness at some follower angles is shown Fig. 2 (right). Observe that it rises exponentially as the deflection increases. The same phenomenon of the tangential force, which reduces the stiffness variation efficiency, is described also in [7]. To reduce its effect, the mechanism is there limited to a lower deflection angle of about ± 15 deg, where the follower torque is lower, to effectively reduce the tangential force.

2.3 RED WORKSPACE REGION

The RED region, as seen in Fig. 2, is created because the stiffness motor has limited torque capabilities. Two things can happen, when the actuator falls into that region, where the torques are higher as the maximum gearbox torques of the stiffness variation motor. In the first case, the stiffness variation motor retains its position, due to the additional friction in its planetary gearbox (gearbox max efficiency 75%), but does not move when commanded. The second case is, when the follower torque is so extreme, that the motor gets backdriven into a lower stiffness position. The mechanism deflection then hits its maximum, since the external torque remains unchanged and the stiffness decreased. This is considered as worse, compared to the first case.

There are several ways to avoid this situation. It could be prevented by utilizing a non-backdrivable gearbox transmission, e.g. the worm gear. However, due to the exponential torque rise, the maximum torques are quite high. A suitable worm-gearbox would be too big and would not improve the efficiency of the system.

Another solution would be to use a ballscrew as a linear motor, which in its size is more tolerable to high forces. The required peaks would then be provided by the motor, which would presumably operate in its short-term region to supply the needed peak torques.

Yet another alternative is to use a stronger stiffness variation motor, however this is in contradiction to initial goals, since a bigger motor increases the device's weight and price.

While the above solutions would improve the functionality of the device, the energy efficiency of the stiffness variation would remain the same. Therefore, a modification is proposed, where a second elastic element is used and the follower helping torque is generated from the external deflection. Using it in this way, the same motor can remain and the torque requirements decrease. This modification is explored in this paper.

3 THE PROPOSED MODIFICATION

3.1 A SECOND SPRING

As seen in Fig. 3a, the prototype is dimensioned through two cam curve parameters ($R_{\rm s}$ and $R_{\rm b}$). Internally, a linear spring with stiffness $k_{\rm lin1}$ is used. Other parameters are more general to a variable stiffness actuator. The reader is referred

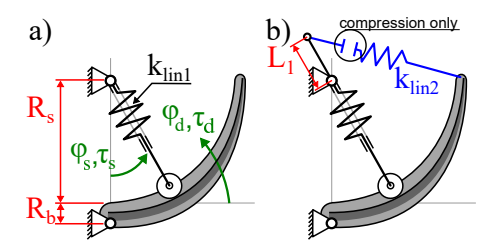


Figure 3 Flat view with the essential parameters describing the original mechanism (a) and the modified in (b).

to [3], which provides a more detailed explanation regarding different general VSA parameters. The present work analysis is done for a deflection range of $\pm 20^{o}$ and for a follower angle range of $0^{o} - 90^{o}$.

As seen in Fig. 3b, the original mechanism is extended through the linear spring (k_{lin2}) connected to the follower at a distance of L_1 . The parameters k_{lin2} and L_1 will be later chosen for optimal performance.

As already mentioned, the mathematical model data is borrowed from [16]. The data corresponds to an actual physical prototype build to test the PLVL variable stiffness mechanism. In the same manner the data from real motors and their nominal/peak gearbox is collected. All parameters used in this article are gathered in Table I.

This second spring is on one end fixed to the curved arm and on the other end connected to the follower through a free connection. This means that the spring can be compressed but not extended. The extension is thus prevented through the spring lift off. No negative deflection torque can occur in such a way, when the follower rotates. This is also clearly marked in 3b as compression only. The second spring thus provides the torque needed to compensate the stiffness variation torque directly from the external deflection of the mechanism.

Conveniently, the follower torque is higher at lower follower angles, where the mechanism's deflection is higher. In contrast, the follower torque is lower at higher follower angle setups, where the mechanism's deflection is lower. The analytical model of the original torque/deflection characteristic was derived in [16], but a shortened derivation can also be found in the APPENDIX A. This work evaluates, in theory, the potential benefits that the proposed modification would have on the existing actuator prototype. Therefore, the same parameters used to construct the physical prototype, are used in the modification model. Since the modification would require a partial redesign of the existing prototype, it will not be realized in this current article.

3.2 NEW MATHEMATICAL MODEL

The modification relies on the previous design from [16]. The main relation used are $\tau_{d,F1}(\varphi_d, \varphi_s, R_s, R_b)$ (36) as the torque at a specific φ_d , φ_s , R_s and R_b . The torque required

to hold a given stiffness is calculated as $\tau_{d,F1}(\varphi_d, \varphi_s, R_s, R_b)$ (39) and is dependent on the same values. More about the derivation of these equations is written in the APPENDIX A. One difference to the work in [16] is in that we use the subscript F1 to represent the original mechanism. In the same way, we use the subscript F2 to represent the effect of the second spring.

The combined effect or the superposition of both is then written with a subscript (F1, F2). The deflection torque and the stiffness holding torque contribution of the modification is thus written as $\tau_{\rm d,F2}(\varphi_d,\varphi_s)$ and $\tau_{\rm s,F2}(\varphi_d,\varphi_s)$, respectively. The same way, the superposition of both is written as $\tau_{\rm d,F1,F2}(\varphi_d,\varphi_s)$ and $\tau_{\rm s,F1,F2}(\varphi_d,\varphi_s)$, respectively.

Figure 4 shows a flat view of the mechanism with marked vectors and parameters, which are helpful in the mathematical model derivation of the modified design. The

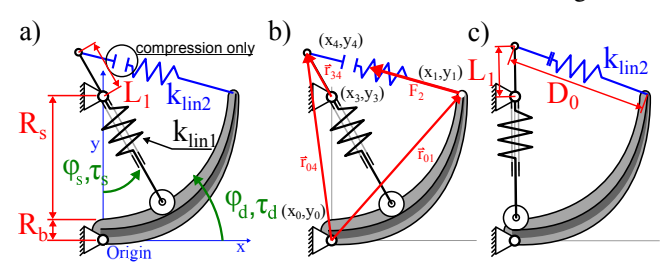


Figure 4 A mechanism's flat view with parameters in (a) and model vectors for calculation of $\tau_{\rm d,F2}$ and $\tau_{\rm s,F2}$ in (b). The unloaded spring F2 is shown in (c).

vector \vec{r}_{01} or the coordinates (x_1,y_1) , which are fixed at the tip of the arc lever. Their value is calculated using (x,y) coordinates from the APPENDIX A as follows:

$$x_{\text{temp}} = x(\varphi_{d} = 0, \, \varphi_{s} = 90^{\circ}, \, R_{s} = 50mm, \, R_{b} = 0),$$
 (1)

$$y_{\text{temp}} = y(\varphi_{d} = 0, \varphi_{s} = 90^{\circ}, R_{s} = 50mm, R_{b} = 0).$$
 (2)

The follower angle at that point is 90 deg. The attachment point $(x_{\text{temp}}, y_{\text{temp}})$ rotates around the origin when the mechanism is deflected and produces:

$$x_1 = x_{\text{temp}} \cos(\varphi_d) - y_{\text{temp}} \sin(\varphi_d),$$
 (3)

$$y_1 = y_{\text{temp}} \cos(\varphi_d) + x_{\text{temp}} \sin(\varphi_d).$$
 (4)

This connection point is essentially rigidly connected to the end point of the curved lever and rotates with it.

Vector \vec{r}_{04} or coordinate (x_4, y_4) is calculated as:

$$x_4 = L_1 \cos(\pi/2 + \varphi_s),\tag{5}$$

$$y_4 = L_1 \sin(\pi/2 + \varphi_s) + R_s + R_b.$$
 (6)

The point (x_4, y_4) rotates with the follower when the φ_s changes. It is assumed that the spring is unloaded at the follower angle of 0^o , and has a base length of D_0 , as seen in Fig. 4(c). Before calculating the spring force, the distance between the coordinates (x_1, y_1) and (x_4, y_4) needs to be

calculated. Let us define it as:

$$D_{14} = d((x_1, y_1), (x_4, y_4)). (7)$$

 D_0 is calculated in the same manner:

$$D_0 = d((x_1, y_1), (x_4, y_4)), \tag{8}$$

however, in this instance the $\varphi_s = 0$ and $\varphi_d = 0$, as seen in 4(c).

At the present setup, when the follower rotates, the spring does not get extended but lifts off. Consequently, the spring force magnitude is calculated as:

$$F2 = \begin{cases} k_{lin2}(D_0 - D_{14}) & \text{if } D_{14} < D_0, \\ 0 & \text{if } D_{14} \ge D_0, \end{cases}$$

representing the cases of compression and the corresponding force, and the case of lift-off with a zero force. The direction of \vec{F}_2 vector is then determined using the basis vectors \vec{r}_{04} and \vec{r}_{01} .

The additional deflection torque due to the modification, i.e. F2, is calculated as:

$$\vec{\tau}_{\text{d,F2}} = \vec{r}_{01} \times \vec{F}_2. \tag{9}$$

The third dimension is then the scalar value $\tau_{d,F2}$. The contribution, i.e., reduction, of the stiffness holding torque (follower torque), due to the modification F2 is calculated as:

$$\vec{\tau}_{\text{s,F2}} = \vec{r}_{34} \times \vec{F}_2. \tag{10}$$

Again, the third dimension is the scalar value $\tau_{s,F2}$. The vector \vec{r}_{34} is calculated as:

$$x_{34} = L_1 \cos(\pi/2 + \varphi_{\rm s}),\tag{11}$$

$$y_{34} = L_1 \sin(\pi/2 + \varphi_{\rm s}). \tag{12}$$

The exact stiffness of the mechanism (K_i) in all cases, is calculated using a derivative between the deflection torque and the deflection angle:

$$K_i = \frac{d\tau_{d,i}}{d\varphi_d}, \text{ where } i \in \{(F1), (F2), (F1,F2)\}.$$
 (13)

The summation of the contributions of both cases is straightforward both for the deflection torque ($\tau_{d,F1,F2}$) and the stiffness holding torque ($\tau_{s,F1,F2}$):

$$\tau_{d,F1,F2} = \tau_{d,F1} + \tau_{d,F2},$$
(14)

$$\tau_{s,F1,F2} = \tau_{s,F1} + \tau_{s,F2}.$$
 (15)

4 PARAMETER OPTIMIZATION

4.1 OPTIMIZATION GOAL

The optimization goal is easily explained using the torque/deflection space of the actuator, as seen in Fig. 5(left). The ideal mechanism would have a stiffness ranging from

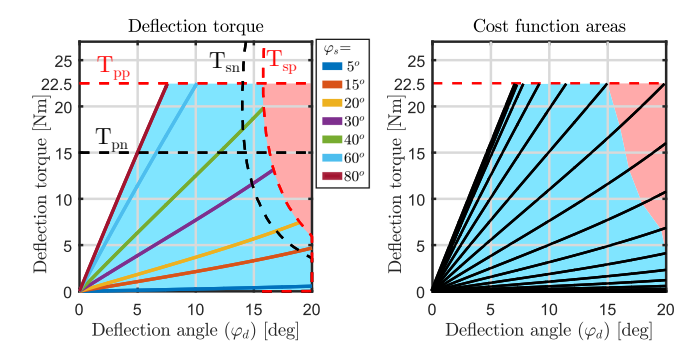


Figure 5 Torque/deflection space (left) and a numerical representation (right).

0 Nm/rad to infinite. In this case, it would fill the whole torque/deflection space. Due to the mechanical limitations and torque limits, the torque/deflection is not completely filled and is split in three regions (BLUE, RED and WHITE), as already previously touched upon. The goal of the optimization is to find a combination of L_1 and k_{lin2} , that reduces the RED area while keeping the BLUE functional area as large as possible. Note that due to the modification, the WHITE area appears also below the torque/deflection lines and rises with the increase in values L_1 and k_{lin2} .

In short, the BLUE region represents the normal operation area of the mechanism. The RED region represents the area, where the stiffness variation motor torque exceeds its gearbox limits and where, in a way, the variable stiffness mechanism loses its functionality. The WHITE are represents the in-accessible region, either due to the backdrivability of the position motor, or the addition of the spring, as it will be later shown.

The maximum torque of the mechanism is limited by the maximum torque of the position motor gearbox (set at 22.5Nm). The parameters T_{pn} , T_{pp} , T_{sn} and T_{sp} represent the limits of the position motor's and stiffness varying motor's gearboxes. Their values can be found in Table I. These parameters limit the torque/deflection space of the actuator. To calculate the boundary lines, torque/deflection lines and stiffness variation motor torques are calculated for a small enough set of discrete follower angles. Each line is then numerically trimmed by the torque limits of both the position motor and the stiffness variation motor. The final lines, representing the boundaries, are then drawn as dashed in Fig. 5. The stiffness motor torque is then non-linearly transformed into the torque/deflection space, again using numerical means.

Since the mechanism's operation principle is not completely perpendicular, the stiffness varying motor does need some torque to hold its position. The RED area shows where the torque required to hold the desired stiffness exceeds the maximum allowable torque of the stiffness varying motor gearbox. The WHITE areas are theoretically inaccessible, and therefore ignored.

4.2 COST FUNCTION

The cost function δ is calculated as the difference between the size of the BLUE area and the size of the RED area as follows:

$$\delta = A_{BLUE} - n \cdot A_{RED},\tag{16}$$

In short, the larger the BLUE area compared to the ideal case, the better δ . In this way, the increase of BLUE area brings us closer to the ideal mechanism. The decrease of the RED area reduces the peak torques of the stiffness variation motor. The cost function δ , is indirectly affected by the stiffness range, the amount of stored energy (surface below torque/deflection curves) and the stiffness variation torque. The first two should be maximized and the last one minimized. The workspace is then limited by the torque limits of the gearboxes of both motors used. The ideal actuator would fill the complete workspace and be limited by the maximum torque of 22.5Nm and by the maximum deflection of 20 deg. This would mean that the mechanism would have a stiffness range from 0 Nm/rad to infinity. And would not be limited by the torque of the stiffness motor. As such, this ideal case is also used to normalize the calculated areas.

To calculate the areas, one can exploit the fact that at a specific follower angle, the torque/deflection curve can be calculated. Using a small step for the follower angle, its neighbouring line can be found. All the lines are always trimmed by the gearbox limits. To calculate either the BLUE or the RED area, one just sums up the regions between the torque/deflection lines. For each discrete parameter set of k_{lin2} and L_1 , the theoretical model is used to calculate the torque/deflection graphs within the nominal/peak torque limits. The BLUE and RED area sizes are then calculated as explained. Areas values are then collected in a matrix, and can be seen in Fig. 6 as an area plot, where A_{BLUE} and

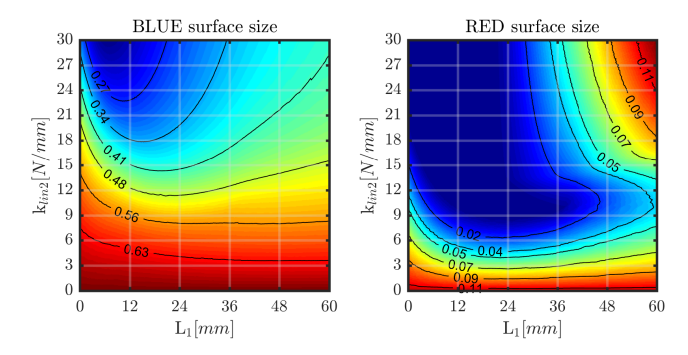


Figure 6 BLUE (left) and RED (right) surface sizes for different k_{lin2} and L_1 parameter combinations.

 A_{RED} represent the normalized BLUE surface size and the normalized RED surface size, respectively. The values are normalized to the full area of:

$$A_i = \max(\varphi_d)T_{pp}$$
, where $i = \{BLUE, RED\}$. (17)

The value of $\max(\varphi_d)=20^o$ and $T_{\rm pp}=22.5Nm$. The surface is then essentially compared to the ideal actuator, where the value would be 1.

The proposed method to find the optimal combination of parameters k_{lin2} and L_1 , is essentially a brute-force search method through all the discrete step combinations. Although other more sophisticated optimization algorithms could be used, it is in this case more valuable to take more time to also visualize the whole parameter area. Additionally, since only 2 parameters are optimized, the brute-force optimization is not yet very computationally demanding. The search is performed for $L_1=0-60mm$ and $k_{lin2}=0-30N/mm$ in dense enough discrete steps. The ranges were determined empirically and since the purpose of this work is to later augment an existing VSA actuator, the parameter boundaries are specified to be physically feasible.

Parameter n is used to weight the importance of both areas. The increase of n increases the impact of the RED area size on the cost value.

The final n value is left to the designer. Consequently, the optimal solution is moving to larger k_{lin2} and L_1 , as seen in Fig. 7. Because the stiffness motor torque lines are non-linearly mapped into the torque deflection space endless increase in the n value does not endlessly improve the cost function, but starts to slowly decrease it. The final n value should be kept as rather smaller than larger.

4.3 COST FUNCTION EVALUATION

Three n values are arbitrarily chosen, i.e., 1, 1.5 and 2. In Fig. 7, the cost function is calculated for these three different n values. In Fig. 7, the optimal value is marked with a red

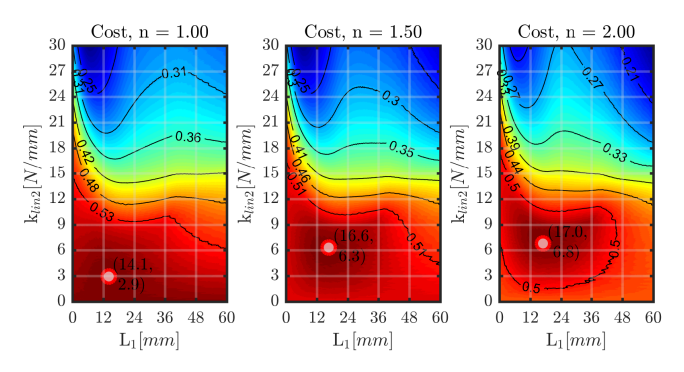


Figure 7 The cost (δ) at different k_{lin2} and L_1 parameter combinations for different n values.

circle for all three cases. The peak values are 0.591 ($L_1 = 14.1$, $k_{lin2} = 2.9$), 0.568 (16.6, 6.3) and 0.558 (17.0, 6.8), for n = 1, 1.5 and 2, respectively. The three peaks move with the change of n, meaning that the optimal combination of parameters also changes. The effect of the value n on the workspace is shown in Fig. 8. As seen in Fig. 8, the addition of a second spring does indeed reduce the size of the RED area, i.e., the condition where the torque required to hold a given stiffness exceeds the peak torque of the stiffness

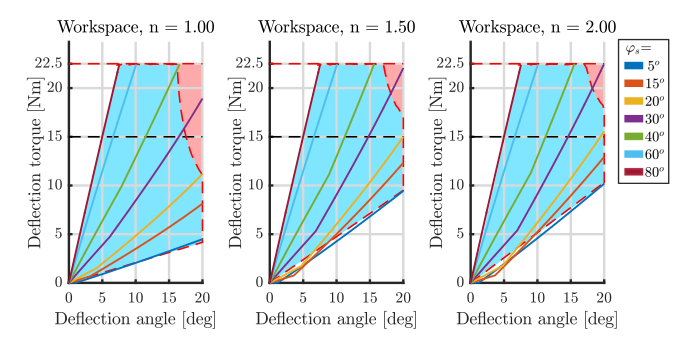


Figure 8 The change of the torque/deflection workspace for different values of n.

holding motor gearbox. However, this also has an effect on the overall size of the BLUE area and consequently also affects the stiffness of the actuator. The final value of the n parameter is left to the designer. In this instance, n=1.5 was arbitrarily chosen. The optimal values for k_{lin2} and L_1 are thus 6.3N/mm and 16.6mm, respectively. The choice of n is justified, since the RED area is completely above the position motor's nominal torque limit (T_{pn}) of 15Nm.

4.4 LINEAR STIFFNESS APPROXIMATION

Before continuing with the comparison between the original and the modified mechanism, the concept of the pseudolinearity needs to be further explained. The linear approximation is in this case important, since it provides a baseline for comparison between both mechanisms. The pseudo-linear property of the original actuator is exploited as in the original work [16] and the slightly nonlinear, i.e., slightly curved, torque/deflection curves are replaced with their respective linear approximations. Consequently, each follower angle now represents one linear approximate It is assumed that a linear approximation stiffness. of stiffness curves sufficiently describes the mechanism response. The dimensionality and complexity of the model are both reduced. This not only simplifies the analysis, but also opens up equal ground for the comparison between the original mechanism and the modified one.

The torque/deflection workspace of the modified mechanism is shown in Fig. 9. As seen, the modified mechanism

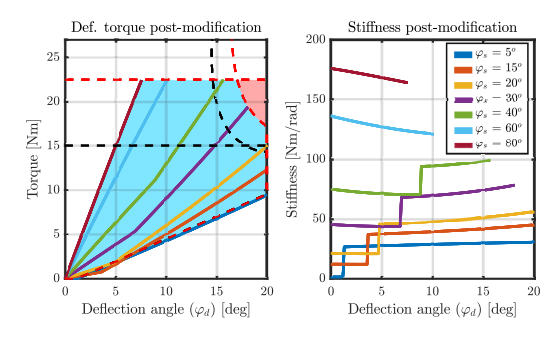


Figure 9 The torque/deflection graph (left) of the modified mechanism and its corresponding stiffness (right).

also exhibits the pseudo-linearity, which is exploited later to represent the mechanism's stiffness through its linear approximation. The linear approximation of each torque deflection curve at a discrete follower angle steps is calculated using a linear regression and the assumption that the lines start at the origin. The linear stiffness approximation is easily calculated by taking the mean of the exact mechanism stiffness, which was calculated numerically from the mechanism's deflection torque.

$$\vec{k}_{\text{approx,F2}} = \text{mean}(K_{\text{F2}}(\vec{\varphi_{\text{d}}}, \ \vec{\varphi_{\text{s}}} = j, \ R_{\text{s}} = 0, \ R_{\text{b}} = 50mm)),$$
(18)

where $\vec{\varphi_s} = j$ is the vector containing the discrete values for follower angles. The linear approximation of the modified mechanism can be seen in 10(left) for a few follower angles. The mean is calculated only in the BLUE area, where the

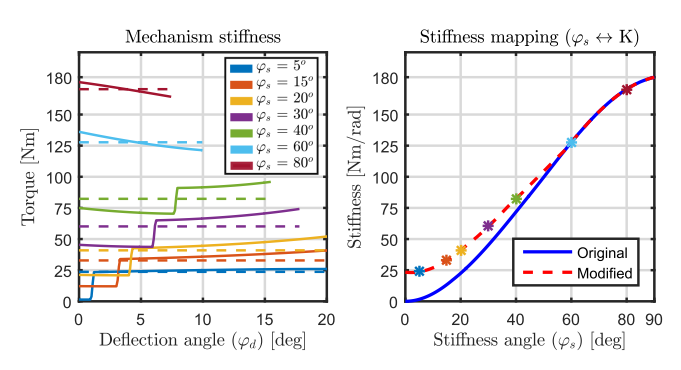


Figure 10 The linear approximation of the modified mechanism(left) and the stiffness mapping between both cases (right).

torques of both motors are below peak limits. The values above peak conditions are ignored. The same process is also used in [16].

One drawback of the modification is the introduced discrete nonlinearity that appears when deflection arm touches the additional spring. This also affects the stiffness of the mechanism and creates a non-linear jump. This is a disadvantage and a side effect of the proposed modification. In Fig. 11(right), the discrete step in the mechanism's stiffness can also be observed. Nevertheless, as it will be seen later, the modification still introduces other benefits.

By collecting linear approximate stiffness values for different follower angles, the relation between the follower angle and the resulting mechanism's stiffness can be calculated. This is essentially done for case F1 as $\vec{k}_{\rm approx,F1}$ and case F2 as $\vec{k}_{\rm approx,F2}$. Two relations are created, one for the original and one for the modified mechanism. The relations for both cases are shown in Fig. 10(right).

One can clearly observe that the stiffness of the modified mechanism is now different, when using the follower angle as a baseline. Some of the lower stiffness levels are now inaccessible, and the overall stiffness range has changed. The modification's effect is stronger at lower stiffness levels. On higher stiffness levels, due to the rotation of the follower, there is no assistance of the second spring, as initially expected.

The mechanisms can be compared on equal ground by using the linear stiffness approximation values rather than angles of the follower. The linearity error, i.e., difference between the linear approximation and the actual mechanism stiffness is shown in Fig. 11.

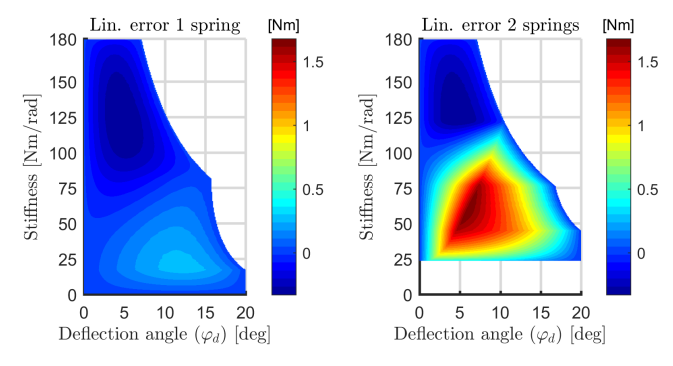


Figure 11 Difference between the actual stiffness and the linear approximation for pre- (left) and post- (right) modification.

One can observe that the torque error is relatively small in the first mechanism. In the modified case, the error increases, however, it is still below reasonable levels.

4.5 ANALYSIS OF THE MODIFICATION'S BENEFITS This section explores how the addition of the second spring affects the torque required to change the stiffness of the motor and the energy required to do so.

The additional spring lever has some slack, which allows the rotation of the follower when a different mechanism stiffness is desired. The slack prevents the generation of a negative torque and ensures that the spring can be compressed only. Through the increase of the follower angle, the slack is increased. The resulting behaviour is that the spring contributes a lot in lower follower angles, i.e., at lower stiffness and less at higher follower angles, i.e., higher stiffness. When the deflection link rotates, it first reduces the slack and then starts with the spring compression.

The increase of the deflection torque and the resulting decrease of torque required to hold a given stiffness can be seen in Fig. 12.

As already written, the mechanism's stiffness changes due to the proposed modification. The stiffness of both mechanisms enables us to compare the pre- and post- modification effects of the mechanism on equal ground.

The torque difference ($\Delta \tau_{s,F1,F2}$) of the stiffness varying motor between both cases is calculated as:

$$\Delta \tau_{s,F1,F2} = \tau_{s,F1,F2} - \tau_{s,F1}.$$
 (19)

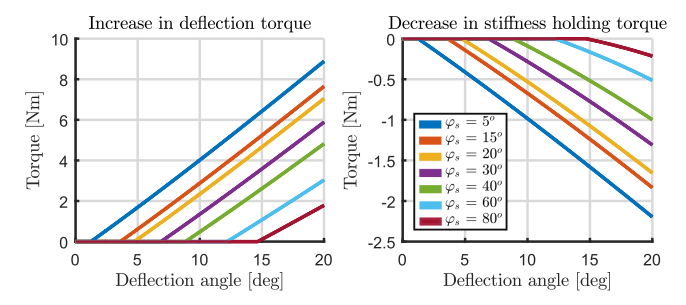


Figure 12 The increase of the deflection torque (left) and the resulting stiffness helping torque (right).

Here, the $\tau_{s,F1,F2}$ represents the stiffness holding torque for the modified mechanism while $\tau_{s,F1}$ represents the stiffness holding torque of the original mechanism. The energy required to change from the minimal to a given stiffness is calculated through the following equation:

$$E_{\mathrm{s,i}} = \int_{\varphi_{\mathrm{s,min}}}^{\varphi_{\mathrm{s}}} \tau_{\mathrm{s,i}} \left(\varphi_{\mathrm{s,i}}(k), \varphi_{\mathrm{d}} \right) d\varphi_{\mathrm{s}}, \text{ where } i \in \left\{ (\mathrm{F1,F2}), \mathrm{F2} \right\},$$

where $\tau_{s,i}$ and the deflection of the external link (φ_s) and the deflection of the external link (φ_d) , for the case of the original mechanism (i=F1) and the modified version (i=(F1,F2)). $\varphi_{s,i}(k)$ represents the relation between the linear stiffness approximation and the follower angle. To compare everything on equal grounds, the results gathered for different follower angles (φ_s) need to be re-mapped to the equivalent stiffness, shown in Fig. 10(right). The minimum stiffness $(\varphi_{s,min})$ is set to 23.2 Nm/rad, since it is the minimum stiffness of the modified mechanism. The difference between the energies required to vary the stiffness in both cases is then calculated as:

$$\Delta E_{\rm s} = E_{\rm s,F1,F2} - E_{\rm s,F1}.\tag{21}$$

The stiffness variation energy result is presented in Fig. 13.

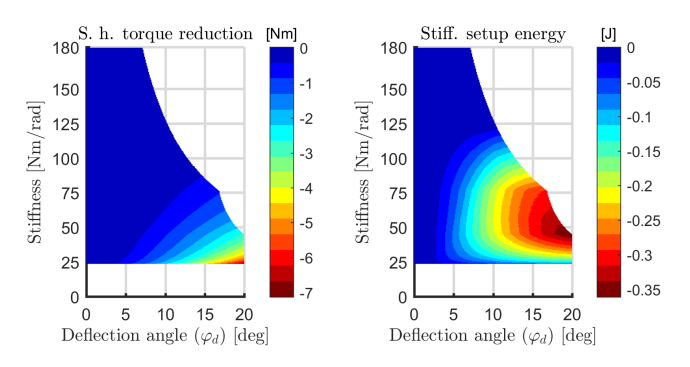


Figure 13 The difference between both mechanism cases for the follower torque, i.e. the torque required to change stiffness (left) and energy (E_s) required for it (right)

From the results, one can again observe in Fig. 13(left), that the torque needed to vary the stiffness at higher deflection angles is lower.

While at a higher stiffness it stays the same as in the original. However, in this graph over the full deflection and full stiffness range, the whole picture is created. Similarly, one can observe, that less energy is needed to vary the stiffness again at low follower angles, i.e., lower stiffness in Fig. 13(right). Through the help of linear stiffness approximation, both mechanism cases can be compared on the same graphs, as seen in Fig. 14. One can see, that the system still

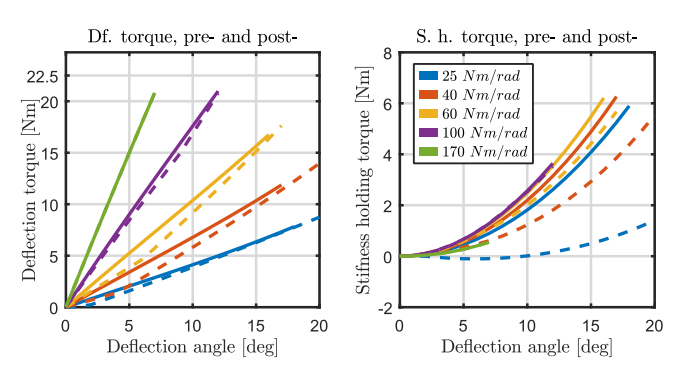


Figure 14 Comparison of torque/deflection graph for different stiffness pre-sets and the torque required to hold the given stiffness, for original and modified mechanism. The solid lines represent the original and the dashed lines the modified mechanism.

preserves the pseudo-linearity, which is favourable from the control's perspective. The deflection range is limited to 20 deg, since the goal of this modification is to improve the actuator developed in [16]. The follower torque, required to change the stiffness, is shown in right graph of Fig. 14. As predicted, due to the modifications, the new follower torque is lower in critical cases. This shows that the proposed modification increases the performance of the device while the same motors are used as in the original concept. Since the motors contribute a lot to the weight of the overall system, keeping the motors small also helps keeping the overall device light, small and compact.

Another important aspect of the mechanism is the amount of elastic energy that is stored in the compressed mechanism. This stored elastic energy should not be confused with the energy required to change a given stiffness. The amount of elastic energy stored in the device is compared for both the pre- and post-modification cases. Generally, more stored energy means a higher possibility for more efficient movement of the external link. The stored **el**astic energy $(E_{\rm el,i})$ is numerically calculated using the equation

$$E_{\mathrm{el,i}} = \int_{\varphi_{\mathrm{d}}=0}^{\varphi_{\mathrm{d}}} \tau_{\mathrm{d,i}} \left(\varphi_{s,i}(k), \varphi_{\mathrm{d}} \right) \mathrm{d}\varphi_{\mathrm{d}}, \quad \text{where } i \in \left\{ (\mathrm{F1,F2}), \mathrm{F2} \right\}. \tag{22}$$

The $\tau_{\rm d,i}$ is the deflection torque dependent on the external link deflection $\varphi_{\rm d}$ and devices stiffness k, dependent on the follower angle $\varphi_{\rm s}$. The results are presented in Fig. 15. Since

the workspaces below the peak torque limits do not perfectly overlap, it is assumed that there is no stored energy if the workspaces overlap but one mechanism case cannot reach it. While the areas where the workspace is unreachable for both cases are ignored, i.e., white in this case.

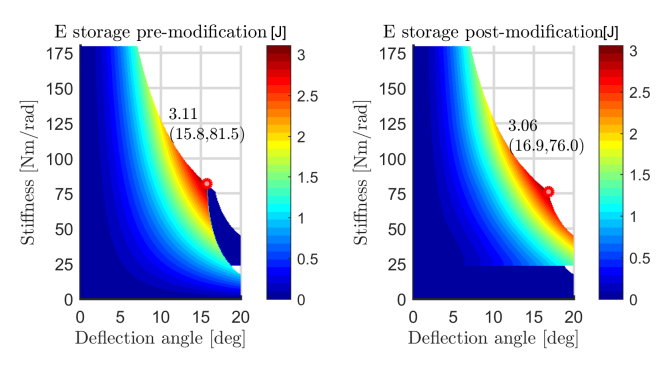


Figure 15 Graphs representing elastic energy storage capacity (left)pre-, (right) post-modification.

One can see that the amount of stored energy does not noticeably change for the maximum deflection of the mechanism of 20 deg. The modified mechanism is able to store more energy in stiffness setups below 75 Nm/rad, compared to the original mechanism. Since the workspaces differ between both versions, a simple difference calculation between them is not sufficient. Therefore, it was omitted. For higher elastic energy storage benefits, the deflection range would need to be increased.

5 CONCLUSION

The addition of a second spring decreases the rising follower torque at lower stiffness pre-sets and at higher deflection angles. The resulting device uses less torque and energy to change its stiffness. The proposed modifications extend the devices torque/deflection workspace, while keeping a slightly smaller stiffness range, but while using the same motors.

As a drawback, the modification both introduces a discrete nonlinearity and reduces the pseudo-linearity of the torque-deflection graph. The lower stiffness levels are also disabled. Although it is unclear how this discrete nonlinearity would affect the performance of an actual physical prototype, at the present stage, this was not explored. Still, the mechanism could find use in applications, where very precise torque measurement is not needed, while still being advantageous if the stiffness can be adapted. Overall, the performance improvement of the stiffness variation mechanism is substantial, which also points at the possibility that other more efficient variable stiffness mechanism architectures could still exist. This will be explored in future work.

REFERENCES

- [1] Albu-Schäffer A., Eiberger O., et al., Soft robotics. *IEEE Robotics & Automation Mag.*, Vol. 15, No. 3, pp. 20-30, 2008.
- [2] Pratt G. A. and Williamson M. M., Series elastic actuators. 1995 IEEE/RSJ International Conference on Intelligent Robots and Systems 95. 'Human Robot Interaction and Cooperative Robots', Vol. 1, pp. 399-406, 1995.
- [3] Wolf S. and Grioli G. et al., Variable Stiffness Actuators: Review on Design and Components. *IEEE/ASME Transactions on Mechatronics*, Vol. 21, No. 5, pp. 2418-2430, 2016.
- [4] Vanderborght B., Albu-Schäffer A. et al., Variable impedance actuators: A review. *Robotics and autonomous systems*, Vol. 61, No. 12, pp. 1601-1614, 2013.
- [5] Tagliamonte N. L., Sergi F. et al., Double actuation architectures for rendering variable impedance in compliant robots: A review. *Mechatronics*, Vol. 22, No. 8, pp. 1187-1203, 2012.
- [6] Van Ham R. and Sugar T. et al., Compliant actuator designs. *IEEE Robotics and Automation Mag.*, Vol. 16, No. 3, pp. 81-94, 2009.
- [7] Jafari A. and Tsagarakis N. G. and Caldwell D. G., A novel intrinsically energy efficient actuator with adjustable stiffness (AwAS). *IEEE/ASME Transactions on Mechatronics*, Vol. 18, No. 1, pp. 355-365, 2013.
- [8] Grebenstein M. and Albu-Schäffer A. et al., The DLR hand arm system. *IEEE International Conference on Robotics and Automation (ICRA)*, Shanghai, China, Vol. 1, pp. 3175-3182, 2011.
- [9] Haldane D. W., Plecnik M. M., Yim J. K. and Fearing R. S., Robotic vertical jumping agility via series-elastic power modulation. *Science Robotics*, Vol. 1, No. 1, 2016.
- [10] Kim, B., Deshpande A. D., Design of nonlinear rotational stiffness using a noncircular pulley-spring mechanism. *Journal of Mechanisms and Robotics*, Vol. 6, No. 4, 2014.
- [11] Dežman, M., Babič J. and Gams A., Qualitative Assessment of a Clutch-Actuated Ankle Exoskeleton. *International Conference on Robotics in Alpe-Adria Danube Region*, Turin, Italy, Vol. 1, pp. 778-786, 2017.
- [12] Maurice P., Čamernik J. and Gorjan D., Schirrmeister B., Bornmann J., Tagliapietra L., Latella C., Pucci D., Fritzsche L., Ivaldi S., Babič J., Objective and Subjective Effects of Passive Exoskeleton on Overhead Work. (Status: submitted).
- [13] Alabdulkarim S., Nussbaum M. A., Influences of different exoskeleton designs and tool mass on physical demands and performance in a simulated overhead drilling task. *Applied ergonomics*, Vol. 74, pp. 55-66, 2019.

- [14] Huysamen K., Bosch T., de Looze M., Stadler K. S., Graf E., O'Sullivan L. W., Evaluation of a passive exoskeleton for static upper limb activities. Applied ergonomics, Vol. 70, pp. 148-155, 2018.
- [15] Dežman M., Gams A., Pseudo-linear variable lever variable stiffness actuator: Design and evaluation. 2017 IEEE International Conference on Advanced Intelligent Mechatronics (AIM), Vol. 1, pp. 785-790, 2017.
- [16] Dežman M. and Gams A., Rotatable cam-based variable-ratio lever compliant actuator for wearable devices. Mechanism and Machine Theory, Vol. 130, pp. 508-522, 2018.
- [17] Vanderborght B., Tsagarakis N. G., MACCEPA 2.0: compliant actuator used for energy efficient hopping robot Chobino 1D. Autonomous Robots, Vol. 31, No. 1, pp. 55-65, 2011.
- [18] Shepherd M. K., Rouse E. J., Design of a quasipassive ankle-foot prosthesis with biomimetic, variable stiffness. IEEE International Conference on Robotics and Automation (ICRA), Singapore, Vol. 1, pp. 6672-6678, 2017.
- [19] Petit F. P., Analysis and control of variable stiffness robots. Doctoral Thesis, ETH-Zürich, 2014

APPENDIX A

The equations and relations required throughout of the manuscript are gathered here in order to increase the readability of the manuscript. For a more detailed derivation of equations, the reader is referred to [16].

In Fig. 16, the mechanism is presented in a flat form.

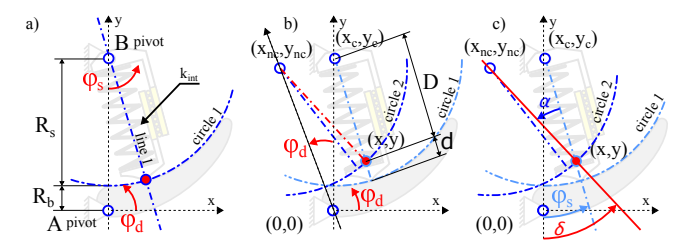


Figure 16 The relevant parameters of the original mechanism are shown in a). In a deflected state b), the rotation of the arc lever (circle 1), is shown **b**) creates an intersection point (red dot) with the red line c). Red line is perpendicular to the deflected circular arc (circle 2) and goes through the center of the circular arc. The pressure angle (α) can be calculated using the inclination (δ) .

The intersection (x,y) between (circle 2) and the red line is calculated as follows (a is introduced to shorten them):

$$x(\varphi_{\mathsf{d}}, \varphi_{\mathsf{s}}, R_{\mathsf{s}}, R_{\mathsf{b}}) = (R_{\mathsf{b}} + R_{\mathsf{s}}) \sin(\varphi_{\mathsf{s}}) \left(2 \sin\left(\frac{\varphi_{\mathsf{d}}}{2}\right) \sin\left(\frac{\varphi_{\mathsf{d}}}{2} - \varphi_{\mathsf{s}}\right) + \mathbf{a}\right)$$
 angle, since when the spring is not completely perpendicular to the load. The amount of elastic energy stored in the

$$y(\varphi_{\rm d},\varphi_{\rm s},R_{\rm s},R_{\rm b}) = (R_{\rm b}+R_{\rm s})\cos(\varphi_{\rm s})\left(\cos\left(\varphi_{\rm d}-\varphi_{\rm s}\right) + \frac{\sin^2(\varphi_{\rm s})}{\cos\left(\varphi_{\rm s}\right)} - \mathbf{a}\right), \\ (24) \qquad E_{\rm el,Fl} = \int_0^{\varphi_{\rm d}} \tau_{\rm d,Fl} \mathrm{d}\varphi_{\rm d}.$$

$$\mathbf{a} = \sqrt{\frac{R_s^2}{(R_s + R_b)^2} - \left(\sin(\varphi_d - \varphi_s) + \sin(\varphi_s)\right)^2}.$$
 (25)

The force is generated by the spring, which lies on the line with an inclination dependent on the φ_s . The compression d is calculated via the distance D. (see Fig. 16(b)) This is then used to estimate the spring force (F_{spr}) :

$$D = \sqrt{(x - x_c)^2 + (y - y_c)^2},$$
(26)

$$d = R_{\rm s} - D, (27)$$

$$F_{\rm spr} = k_{\rm int} d. \tag{28}$$

To calculate the pressure angle(α), line 1 and the deflected circle 2 (φ_d) can be used for this (note that $x_c = 0, y_c =$

$$x_{\rm nc} = x_{\rm c}\cos(\varphi_{\rm d}) - y_{\rm c}\sin(\varphi_{\rm d}),\tag{29}$$

$$y_{\rm nc} = y_{\rm c}\cos(\varphi_{\rm d}) + x_{\rm c}\sin(\varphi_{\rm d}),\tag{30}$$

$$\delta = \arctan\left(\frac{y - y_{\rm nc}}{x - x_{\rm nc}}\right) + \frac{\pi}{2},\tag{31}$$

$$\alpha = \delta - \varphi_{\rm s}.\tag{32}$$

Through the rotation/deflection (φ_d) of the original circle center (x_c, y_c) , the new circle center coordinates (x_{nc}, y_{nc}) are calculated. The line going through (x, y) and (x_{nc}, y_{nc}) has an inclination of δ . It is perpendicular to the lever, i.e., it goes through the rotated circle center. It is needed to calculate the pressure angle (α). The $\pi/2$ in (31) represents the complementary angle. Using vector cross product, the deflection torque ($\tau_{d,F1}$):

$$F = F_{\rm spr}/\cos(\alpha),\tag{33}$$

$$\vec{F} = F\left[\cos\left(-\pi/2 + \varphi_{s} + \alpha\right), \sin\left(-\pi/2 + \varphi_{s} + \alpha\right), 0\right],\tag{34}$$

$$\vec{r} = [x, y, 0] \tag{35}$$

$$\vec{\tau}_{d,F1}(\varphi_d, \varphi_s, R_s, R_b) = \vec{r} \times \vec{F}.$$
(36)

The third dimension of the vector $\vec{\tau}_{\mathrm{d},F1}$ can be then directly used as $\tau_{d,F1}$ in the equations that follow. analytical stiffness is calculated using the derivative or, more practically, using numerical approximation methods:

$$K_{F1} = \frac{\mathrm{d}\tau_{\mathrm{d},F1}}{\mathrm{d}\varphi_{\mathrm{d}}}.\tag{37}$$

At any given state (φ_s, φ_d) , the torque $(\tau_{s,F1})$ required to hold a desired stiffness, angle φ_s , is calculated as

$$F_{\rm din} = F_{\rm spr} \tan(\alpha),\tag{38}$$

$$\tau_{s,F1}(\varphi_d, \varphi_s, R_s, R_b) = F_{din} D. \tag{39}$$

The tangential force (F_{din}) appears due to the rising pressure to the load. The amount of elastic energy stored in the

$$E_{\text{el,F1}} = \int_0^{\varphi_{\text{d}}} \tau_{\text{d,F1}} d\varphi_{\text{d}}.$$
 (40)